Photoelectron recapture and reemission process associated with double Auger decay in Ar

Y. Hikosaka,[1] R. Mashiko,[2] T. Odagiri,[3] J. Adachi,[4] H. Tanaka,[4] T. Kosuge,[4] and K. Ito[4]
[1]*Graduate School of Medicine and Pharmaceutical Sciences, University of Toyama, Toyama 930-0194, Japan*
[2]*Department of Environmental Science, Niigata University, Niigata 950-2181, Japan*
[3]*Department of Materials and Life Sciences, Sophia University, Tokyo 102-8554, Japan*
[4]*Photon Factory, Institute of Materials Structure Science, Tsukuba 305-0801, Japan*
(Received 21 April 2016; published 14 June 2016)

Multielectron coincidence spectroscopy has been performed for Ar at a photon energy of only 0.2 eV above the $2p_{1/2}$ threshold. It is revealed that a postcollision interaction induced by double Auger decay leads to photoelectron recapture, followed by reemission of the captured electron, where the recapture of the slow photoelectron forms the Ar^{2+} Rydberg-excited states which subsequently undergo autoionization. The energy correlation of the emitted electrons discloses that both direct and cascade paths in the double Auger decay contribute to the photoelectron recapture.

DOI: 10.1103/PhysRevA.93.063412

I. INTRODUCTION

Inner-shell photoionization of an atom in the ionization threshold region results in the emission of a slow photoelectron, and a subsequent Auger decay of the formed core-hole state can thus occur when the photoelectron is still in the atomic field. Here, a postcollision interaction (PCI), the Coulomb interaction among the photoelectron, the Auger electron(s), and the atomic field changing during Auger decay, plays a significant role, and leads to an energy loss of the photoelectron and the corresponding energy gain of the Auger electron(s). When the photon energy approaches close to the ionization threshold and accordingly the photoelectron escapes initially with a low kinetic energy, the energy loss of the photoelectron due to PCI can be larger than the initial kinetic energy in the photoionization process. In this case, the outgoing photoelectron is recaptured into a high-n Rydberg orbital [1].

For the dominant Auger decay pathway emitting a single Auger electron, the associated photoelectron recapture produces a singly charged ion in a high-n Rydberg state. If the high-n Rydberg state lies above the double-ionization threshold, the recaptured photoelectron can be reemitted through autoionization [2]. The autoionization lines corresponding to such photoelectron reemission processes have been identified generally in electron spectra measured around atomic inner-shell thresholds [3–6]. Moreover, related processes are observed for molecules, where singly charged molecular ions formed by the photoelectron recapture undergo dissociation and a subsequent electron emission occurs from the dissociation fragments [7,8].

Besides single Auger electron emission, double Auger decay in which two Auger electrons are emitted contributes also for a significant fraction in the total Auger intensity. For example, the Auger decay of the Ar $2p$ holes includes a 10% contribution of double Auger decay [9]. The PCI associated with double Auger decay may also induce photoelectron recapture followed by reemission, where autoionizing doubly charged ion states are produced intermediately. No direct evidence of such a process, however, has been obtained so far for atoms. Meanwhile, recently a multielectron coincidence investigation on the inner-shell photoionization of H_2O clarified a related process in which autoionizing fragments are produced by the dissociation of high-lying H_2O^{2+} states [10]. The H_2O^{2+} states are populated by photoelectron recapture associated with double Auger decay.

In this article, we have performed a multielectron coincidence measurement for Ar at a photon energy of only 0.2 eV above the Ar $2p_{1/2}$ threshold. An energy correlation analysis of triple coincidence events enables us to identify the photoelectron recapture and reemission process associated with double Auger decay. It is revealed that, as well as a direct double Auger path in which the two Auger electrons are emitted simultaneously, a cascade double Auger path through the creation and decay of intermediate Ar^{2+} states contributes to the photoelectron recapture.

II. EXPERIMENT

The experiment was performed at the undulator beamline BL-16A of the Photon Factory. The storage ring was operated at the hybrid-fill mode [11] with the bunch filling pattern comprising a train of low-current bunches (350 mA for 156 bunches) and a single high-current bunch (50 mA) diametrically opposite to the bunch train. The single bunch is isolated from the bunch train by symmetrical 156-ns gaps. The stored current was kept constant by top-up injection.

Synchrotron radiation from twin APPLE-II type undulators whose magnetic field conditions were set to be identical was monochromatized by a grazing incidence monochromator using a varied-line-spacing plane grating [12]. A mechanical chopper [13], synchronized to the master clock of the storage ring operation, was used to select the light from the isolated single bunch. The chopper is based on a spinning disk (a diameter of 200 mm) with the rotational axis parallel to the photon beam. At the periphery of the disk, 360 slits of 50 μm (tangential)$\times$1.5 mm (radial) are engraved at equal intervals. The achieved repetition rate of the light pulses from the single bunch is 144 kHz. A simple geometrical estimation assuming a light focal size of 20 μm results in an opening time of 280 ns, which is enough to block fully the light from the bunch train part; at the present measurement setting, however, a leak of the bunch-train light was found to be about 4% in total intensity of the light passing through the chopper.

Multielectron coincidence spectroscopy was performed using a magnetic bottle electron spectrometer [14]. The description of the spectrometer and the data accumulation scheme is given elsewhere [15]. Electrons formed in the ionization region are captured over a 4π solid angle by the magnetic field lines and are guided towards the microchannel plate (MCP) detector terminating a 2.5-m flight path. An acceleration of 100 eV is finally given to electrons before hitting the MCP detector. The flight time of a 0 eV electron is around 4 μs due to a weak electric field applied in the ionization region, and electrons in the whole energy range are detected before the next light pulse. Conversion of the electron time of flight to the kinetic energy was achieved by measuring Ar photoelectron spectral lines at different photon energies. The energy-resolving power of the spectrometer, $E/\Delta E$, was estimated to be nearly constant at 60 for electrons of $E > 3$ eV, though ΔE was limited to around 20 meV [full width at half maximum (FWHM)] for $E < 1$ eV. The electron detection efficiency of the spectrometer was measured as decreasing slowly with electron kinetic energy from 55% ($E = 0$ eV) to 35% ($E = 200$ eV). Electrons produced by the leak of the bunch-train light can be effectively filtered out in the data analysis, since their flight times with respect to the isolated single bunch have offsets and thus their calculated energies are out of the expected energy range.

III. RESULTS AND DISCUSSION

A multielectron coincidence data set for Ar was accumulated at a photon energy of $h\nu = 250.95$ eV for 6 h with a count rate around 4 kHz. The photon bandwidth of the monochromator was set to around 40 meV, and the uncertainty in the photon energy calibration was around ± 30 meV. Figure 1 shows an electron energy spectrum in the kinetic energy range of 0–30 eV, derived from the total events in the coincidence data set. The photon energy is only 2.3 and 0.2 eV above the $2p_{3/2}$ and $2p_{1/2}$ thresholds (248.628 and 250.776 eV [16]), respectively, and thus the photoelectrons are subject to a remarkable PCI effect. In fact, one finds in Fig. 1 that the shape of the $2p_{3/2}$ photoelectron peak is asymmetric with a long tail at its lower kinetic energy side and the maximum is shifted to -0.2 eV from the nominal energy. For the $2p_{1/2}$ photoionization, though only a small fraction of the photoelectron peak can be identified above the kinetic energy of 0 eV, most of the photoelectron intensity has disappeared. In this case, the energy loss due to PCI is principally larger than the kinetic energy gained at the initial photoionization, and the photoelectron is predominantly recaptured into a high-n Rydberg orbital.

For the single Auger decay of the $2p_{1/2}$ core-hole state, the sequential process leading to the photoelectron recapture can be represented as

$$\mathrm{Ar} + h\nu \rightarrow \mathrm{Ar}^{+}2p_{1/2}^{-1} + e_{\mathrm{photo}} \tag{1a}$$

$$\rightarrow \mathrm{Ar}^{2+}3l^{-2} + e_{\mathrm{photo}} + e_{\mathrm{Auger}} \tag{1b}$$

$$\rightarrow \mathrm{Ar}^{+}3l^{-2}\,\mathrm{Ry} + e_{\mathrm{Auger}}. \tag{1c}$$

When the Ar^+ state finally populated by process (1c) is highly excited and lies above the Ar^{2+} threshold, the recaptured photoelectron can be reemitted through autoionization

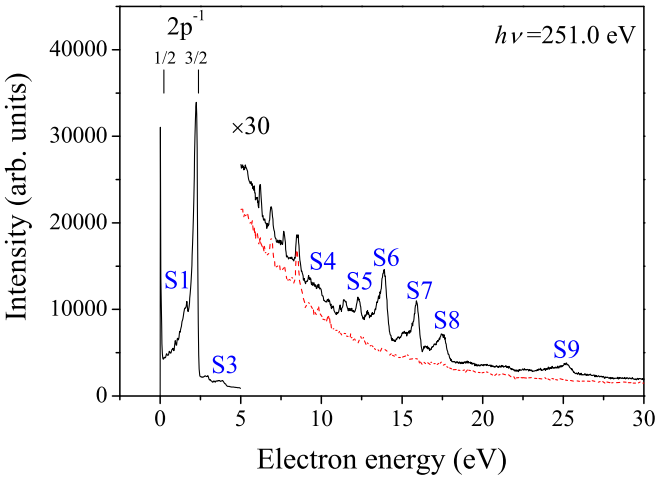

FIG. 1. Kinetic energy spectrum (solid black) of all electrons emitted from Ar ionized at a photon energy of 250.95 eV, which is only 2.3 and 0.2 eV above the $2p_{3/2}$ and $2p_{1/2}$ thresholds, respectively. The nominal kinetic energies of the $2p_{3/2}$ and $2p_{1/2}$ photoelectrons, expected in the absence of PCI, are indicated. The assignments of the photoelectron reemission structures (labeled as S1–S9) associated with the single Auger decay are summarized in Table I of Ref. [6]. Note that structure S2 overlaps the $2p_{3/2}$ photoelectron peak. The dashed red spectrum delineates the contribution from the normal double Auger decay after the $2p$ photoelectron emission, which was obtained in coincidence with the $2p$ photoelectrons in the kinetic energy range of 0–2.5 eV.

of the Ar^+ state:

$$\mathrm{Ar}^{+}3l^{-2}\,\mathrm{Ry} \rightarrow \mathrm{Ar}^{2+}3l^{-2} + e. \tag{2}$$

Figure 1 exhibits peak structures resulting from the photoelectron reemission [process (2)], confirming the previous investigation [6]. Here, the same labels (S1–S9) as in Ref. [6] are adopted to present the structures. Each peak shows an asymmetric shape with a tail toward the lower kinetic energy side, resulting from the overlap of the autoionization lines from the Ar^+ Rydberg series.

Similar to the single Auger decay, the double Auger decay of the $2p_{1/2}$ core-hole state may induce photoelectron recapture followed by reemission:

$$\mathrm{Ar} + h\nu \rightarrow \mathrm{Ar}^{+}2p_{1/2}^{-1} + e_{\mathrm{photo}} \tag{3a}$$

$$\rightarrow \mathrm{Ar}^{3+}3l^{-3} + e_{\mathrm{photo}} + e_{\mathrm{Auger}} + e_{\mathrm{Auger}} \tag{3b}$$

$$\rightarrow \mathrm{Ar}^{2+}3l^{-3}\,\mathrm{Ry} + e_{\mathrm{Auger}} + e_{\mathrm{Auger}}, \tag{3c}$$

and then

$$\mathrm{Ar}^{2+}3l^{-3}\,\mathrm{Ry} \rightarrow \mathrm{Ar}^{3+}3l^{-3} + e. \tag{4}$$

The energy of the electron emitted in process (4) is defined by the energy difference between the high-n Rydberg Ar^{2+} and final Ar^{3+} levels, and is expected to fall mostly within the kinetic energy range shown in Fig. 1; however, any tangible structures associated with the minor Auger pathway are hardly identified in this ordinary electron energy spectrum. Note that this spectrum includes the contribution from the double Auger decay from the $2p^{-1}$ core-hole states formed by the complete ejection of the photoelectron. The contribution, estimated from

the coincidence events including the $2p$ photoelectrons in the kinetic energy range of 0–2.5 eV, is shown by the dashed red curve in this figure, which exhibits the continuous distribution due to the direct path and some sharp peaks due to the cascade processes [17].

The sequence of processes (3) and (4) results finally in emission of three electrons in total (two Auger electrons and an autoionization electron), and thus this sequential process can be isolated by inspecting the triple coincidence events in the coincidence data set. Practically, the triple coincidences include a dominant contribution from the normal double Auger decay of the $2p^{-1}$ core-hole states (triple coincidences of a $2p$ photoelectron and two Auger electrons) [17]; however, its contribution can be effectively excluded by masking the events including an electron in the kinetic energy range of 0–2.5 eV, considering that the photoelectron has a kinetic energy of less than 2.5 eV.

The triple coincidences in which the contribution from the normal double Auger decay of $2p^{-1}$ is thus excluded are displayed in the two-dimensional map in Fig. 2. Here, the coincidence yields are plotted as a function of the sum of the kinetic energies of the two faster electrons (horizontal axis) and of the kinetic energy of the slowest electron (vertical axis). In this way of plotting, the formation of a given Ar^{3+} final state should appear on the diagonal line defined by the equation

$$\begin{aligned}&(\text{Binding energy of } Ar^{3+} \text{ state})\\ &\quad = h\nu - (\text{sum of kinetic energies of two faster electrons})\\ &\qquad - (\text{kinetic energy of slowest electron}).\end{aligned} \tag{5}$$

In practice, several diagonal stripes comprising island structures are identified as the final formations of the $Ar^{3+}\,3p^{-3}$ and $3s^{-1}3p^{-2}$ states. The island structures are attributed to the photoelectron recapture and reemission process associated with the double Auger decay.

The top panel in Fig. 2 shows the projection of the coincidence yields on the two-dimensional map toward the horizontal axis. Assuming that the two Auger electrons emitted in the double Auger decay are faster than the autoionization electron, this projection delineates the populations of the $Ar^{2+}\,3l^{-3}$Ry states produced in process (3c), and is thus plotted as a function of the binding energy of Ar^{2+}, converted by the relation of

$$\begin{aligned}&(\text{Binding energy of } Ar^{2+} \text{ state})\\ &\quad = h\nu - (\text{sum of kinetic energies of two Auger electrons}).\end{aligned} \tag{6}$$

In the projection curve, peaks are observed just below the binding energies of the Ar^{3+} levels. These peaks can be allocated to the high-n Rydberg-excited Ar^{2+} states populated by photoelectron recapture [process (3c)]. This observation justifies the assumption that the electrons emitted by the autoionization [process (4)] are often slowest in the three emitted electrons. Accordingly, the island structures on the two-dimensional map are observed at the vertical locations corresponding to the energies of the autoionization electrons emitted from the high-n Rydberg Ar^{2+} states.

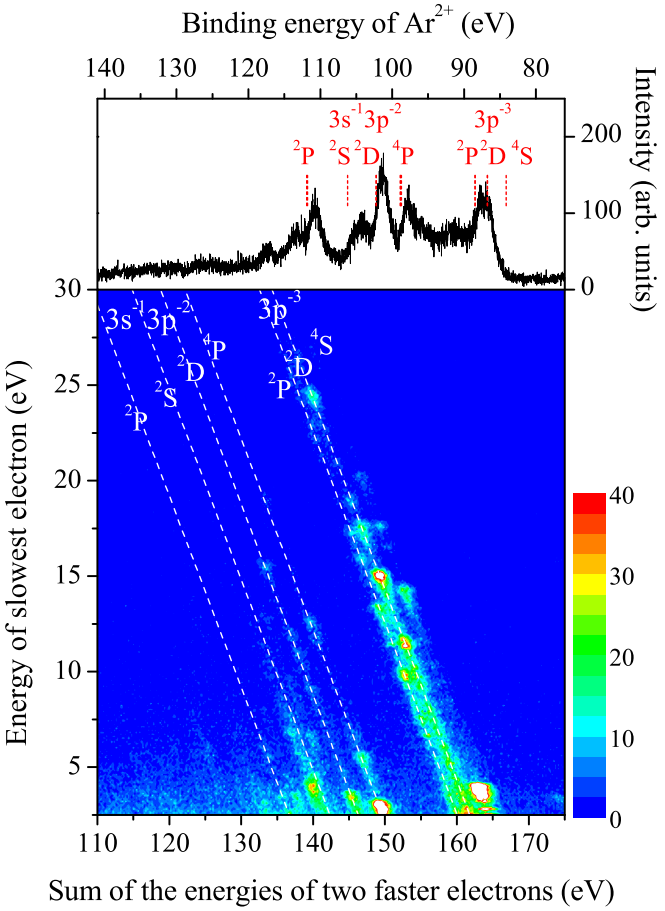

FIG. 2. Energy correlation map plotting triple coincidence yields due to the photoelectron recapture and reemission process associated with the double Auger decay. The top panel shows the projection of the coincidence yields onto the horizontal axis, delineating the Ar^{2+} Rydberg states populated after the photoelectron recapture. The binding energies of Ar^{3+} levels [18] which correspond to the converging limits of these Ar^{2+} Rydberg states are indicated with dotted lines. Note that the Ar^{3+} states with the main configuration of $3p^{-4}3d$, lying densely in 105–115 eV, are not located, in order to avoid congestion.

For a clear display of the autoionization structures, intensity distributions are extracted along the diagonal lines for the formation of the individual $Ar^{3+}\,3p^{-3}$ states, and are plotted in Fig. 3. It is found that the autoionization peak profiles are asymmetric with sharp edges at their higher kinetic energy sides and long tails towards lower-energy sides. The asymmetric profiles result from the overlaps of autoionization lines of Ar^{2+} Rydberg states converging to excited Ar^{3+} levels, and thus reflect the populations of the Ar^{2+} Rydberg states due to the photoelectron recapture. The vertical bars in Fig. 3 indicate the energies [18] of higher-lying Ar^{3+} levels with respect to the individual final Ar^{3+} states, and their locations agree with the edges at the higher kinetic energy sides of the major peak structures. Accordingly, assignments of the peak structures are straightforward: Most of the peaks are assigned to the Rydberg states converging to the $Ar^{3+}\,3s^{-1}3p^{-2}$ levels, while the large peak structure around 4 eV in the formation of $Ar^{3+}3p^{-3}\,^4S$ is allocated to the autoionization from the

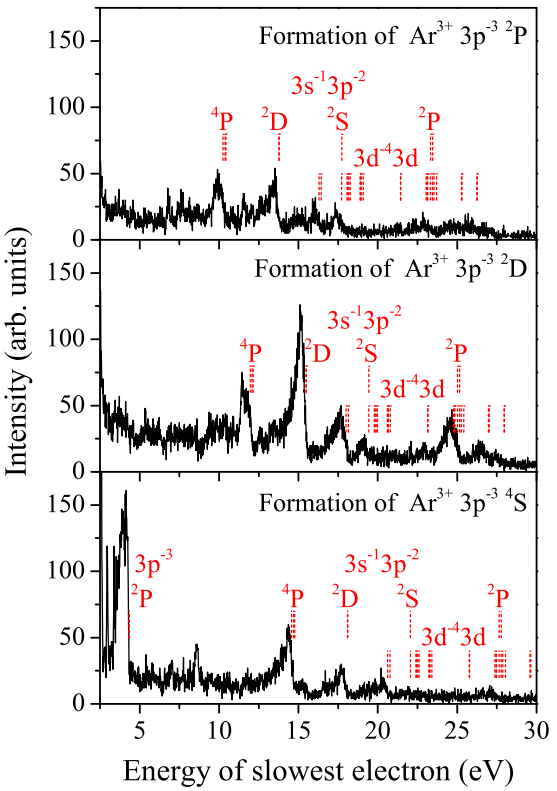

FIG. 3. Energy distributions of the slowest electrons emitted for the final formation of the three components of $Ar^{3+}\,3p^{-3}$, which correspond to the intensity distributions along the diagonal lines in Fig. 2 for the formation of the individual Ar^{3+} states. The spectra delineate the energies of reemission electrons due to autoionization of the Ar^{2+} Rydberg states populated after the photoelectron recapture. The energies [18] of higher-lying Ar^{3+} levels with respect to the individual final Ar^{3+} states are indicated.

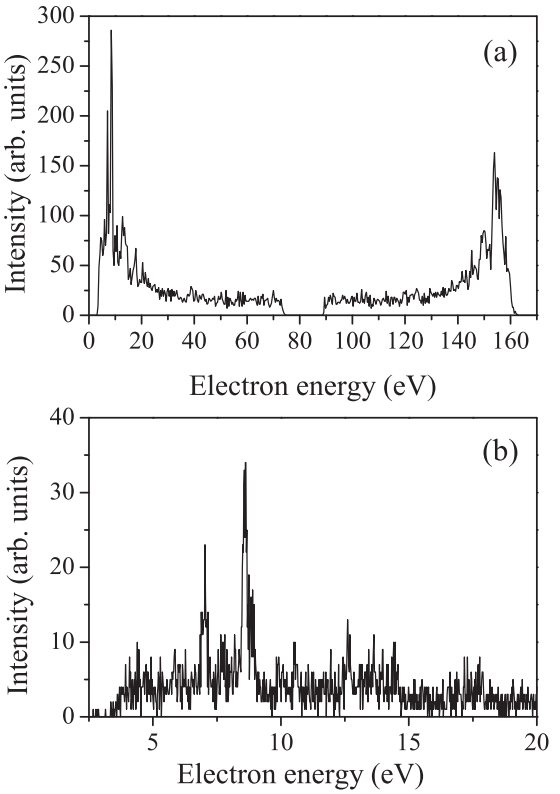

FIG. 4. (a) Energy distribution of the two Auger electrons for the photoelectron recapture into the Rydberg states converging to $Ar^{3+}\,3p^{-3}\,{}^2P$. The first 2.5-eV width spectral range and the corresponding last range are lost by masking the contribution from the double Auger decay of $2p^{-1}$ (see text). The blind range around the middle, where two Auger electrons have almost equal kinetic energies, arise from the detection dead time of 40 ns. (b) Enlargement of the low kinetic energy part of the distribution in (a).

Rydberg states converging to $Ar^{3+}\,3p^{-3}\,{}^2P$. The peaks seen between the Rydberg states converging to the ^2D and ^2S levels of $Ar^{3+}\,3s^{-1}3p^{-2}$ are ascribable to the Rydberg states converging to $Ar^{3+}\,3p^{-4}(^3P)3d\,{}^2P$. It is likely that autoionization from some Ar^{2+} Rydberg states shows strong preferences for the final Ar^{3+} states: For example, autoionization of the Rydberg states converging to $3s^{-1}3p^{-2}\,{}^2D$ forms preferably $3p^{-3}\,{}^2D$, moderately $3p^{-3}\,{}^2P$, and weakly $3p^{-3}\,{}^4S$, while the formation of $3p^{-3}\,{}^2D$ is predominant in the autoionization from the Rydberg states converging to $3s^{-1}3p^{-2}\,{}^2P$.

Next, the pathway of the double Auger decay in process (3b) is considered in detail. The emission of the two Auger electrons occurs simultaneously (direct double Auger decay) or in a stepwise manner through the creation and the decay of an intermediate Ar^{2+} state (cascade double Auger decay) [17]. Both the two Auger electrons emitted in the direct path have continuous energy distributions, while those in the cascade path have discrete energies. These two paths are therefore distinguishable from each other in the inspection of the energy sharing of the Auger electrons.

Figure 4(a) shows the energy distribution of the two Auger electrons emitted for the formation of the Ar^{2+} Rydberg states converging to $Ar^{3+}\,3p^{-3}\,{}^2P$. This plot is derived from the triple coincidences for the formation of $Ar^{3+}3p^{-3}\,{}^4S$ on condition that the two Auger electrons of higher energies are observed in coincidence with an electron of 3–4.5 eV (corresponding to autoionization from the Rydberg states converging to $Ar^{3+}\,3p^{-3}\,{}^2P$). Here, the contribution from the double Auger decay of $2p^{-1}$ is excluded, as mentioned before, by masking the triple coincidence events including an electron in the kinetic energy range of 0–2.5 eV. The energy distribution in Fig. 4(a) generally shows a U-shaped profile, which is commonly observed for the direct path in double Auger decay.

An enlargement of the low kinetic energy part of Fig. 4(a) is shown in Fig. 4(b), where at least two sharp peaks ascribed to the cascade path are visible. Their kinetic energies and the relative intensities agree well with those of the peaks seen in the cascade path of the normal double Auger decay from the $Ar^+\,2p^{-1}$ core-hole states into the final $Ar^{3+}\,3p^{-3}\,{}^2P$ state [17]. The Ar^{2+} states formed intermediately in the normal double Auger decay are assigned to $3p^{-4}3d^2$ [17]. Consequently, the cascade path observed in Fig. 4 is explained as follows. Immediately after the $2p_{1/2}$ photoionization, the cascade double Auger decay proceeds into $Ar^{3+}\,3p^{-3}\,{}^2P$ via intermediate $Ar^{2+}\,3p^{-4}3d^2$ states, and the PCI leads to the photoelectron recapture into the Ar^{2+} Rydberg

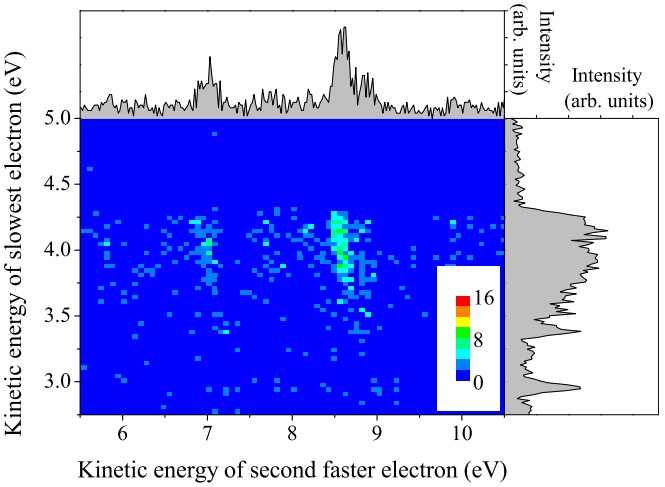

FIG. 5. Two-dimensional map of energy correlation between second faster and slowest electrons emitted for the final formation of $Ar^{3+}3p^{-3}\,{}^4S$, through the photoelectron recapture into the Rydberg states converging to $Ar^{3+}\,3p^{-3}\,{}^2P$. The second faster and slowest electrons correspond practically to the second-step Auger electron in the cascade double Auger decay and the reemission electron, respectively. The top and right panels show the replots of the corresponding ranges of the spectra in Figs. 4(b) and 3 (bottom), respectively.

states converging to $Ar^{3+}\,3p^{-3}\,{}^2P$. Subsequently, the Ar^{2+} Rydberg states formed undergo autoionization into $Ar^{3+}3p^{-3}\,{}^4S$, resulting in the reemission of the recaptured photoelectron. The observation of this sequential process manifests that the lifetimes of the $Ar^{2+}\,3p^{-4}3d^2$ states intermediately formed in the cascade double Auger decay are not long enough to allow the photoelectron to escape fully outside the atomic field.

It is estimated from the intensities of the U-shaped continuum and the peak structures in Fig. 4(a) that the cascade path shares ∼30% in the formation of the Ar^{2+} Rydberg states converging to $Ar^{3+}\,3p^{-3}\,{}^2P$. For the formations of Ar^{2+} Rydberg states converging to the $Ar^{3+}\,3s^{-1}3p^{-2}$ states, the energy distributions of the two Auger electrons (not shown) display similar U-shaped profiles, but no remarkable peak structures assignable to the cascade path are identified in the distributions. This observation is consistent with the fact that the direct path is dominant in the normal double Auger decay of the $Ar^{+}\,2p^{-1}$ core-hole states into $Ar^{3+}\,3s^{-1}3p^{-2}$ [17].

Figure 5 displays the energy correlations between the second-step Auger electron in the cascade double Auger decay (horizontal) and the reemission electron (vertical), for the photoelectron recapture into the Rydberg states converging to $Ar^{3+}\,3p^{-3}\,{}^2P$. Structures corresponding to the cascade double Auger path via the $Ar^{2+}\,3p^{-4}3d^2$ states can be identified on the energy correlation map. The tilted ridges of these structures imply that the energy of the reemission electron decreases as increasing the energy of the second-step Auger electron. In other words, lower-n Rydberg states converging to $Ar^{3+}\,3p^{-3}\,{}^2P$ are produced by a larger energy gain of the second-step Auger electron; this observation is reasonable in terms of the PCI effect. On the energy correlation map, the slopes of the structure ridges are around −3, implying that the energy loss of the photoelectron is about three times larger than the energy gain of the second-step Auger electron. The energy gain of the first-step Auger electron, which cannot be directly detected with the limited energy resolution for such a high-energy range, should balance the excessive energy loss of the photoelectron, and is about two times larger than that of the second-step Auger electron. The energy sharing between the two Auger electrons results from the PCI dynamics reflecting the lifetime of the intermediate Ar^{2+} states.

In conclusion, multielectron coincidence spectroscopy has been performed for Ar at a photon energy close to the $2p_{1/2}$ threshold. The energy correlation information enabled us to isolate the photoelectron recapture and reemission process associated with the double Auger decay, and to reveal that both cascade and direct paths in the double Auger decay contribute to the photoelectron recapture.

ACKNOWLEDGMENTS

We are grateful to the Photon Factory staff for the stable operation of the PF ring. This work was performed with the approval of the Photon Factory Program Advisory Committee (Proposals No. 2013G002 and No. 2015G654).

[1] W. Eberhardt, S. Bernstorff, H. W. Jochims, S. B. Whitfield, and B. Crasemann, Phys. Rev. A **38**, 3808 (1988).
[2] J. A. R. Samson, W. C. Stolte, Z. X. He, J. N. Cutler, and D. Hansen, Phys. Rev. A **54**, 2099 (1996).
[3] R. Hentges, N. Müller, J. Viefhaus, U. Heinzmann, and U. Becker, J. Phys. B **37**, L267 (2004).
[4] A. De Fanis, G. Prümper, U. Hergenhahn, M. Oura, M. Kitajima, T. Tanaka, H. Tanaka, S. Fritzsche, N. M. Kabachnik, and K. Ueda, Phys. Rev. A **70**, 040702(R) (2004).
[5] A. De Fanis, G. Prümper, U. Hergenhahn, E. Kukk, T. Tanaka, M. Kitajima, H. Tanaka, S. Fritzsche, N. M. Kabachnik, and K. Ueda, J. Phys. B **38**, 2229 (2005).
[6] X. M. Feng, A. A. Wills, E. Sokell, T. W. Gorczyca, M. Wiedenhoeft, and N. Berrah, Phys. Rev. A **72**, 042712 (2005).
[7] E. Shigemasa, T Kaneyasu, Y. Tamenori, and Y. Hikosaka, J. Electron Spectrosc. Relat. Phenom. **156–158**, 289 (2007).
[8] T. Gejo, M. Oura, M. Kuniwake, K. Honma, and J. R. Harries, J. Phys.: Conf. Ser. **288**, 012023 (2011).
[9] N. Saito and I. H. Suzuki, J. Phys. Soc. Jpn. **66**, 1979 (1997).
[10] Y. Hikosaka, M. Sawa, M. Nakano, K. Soejima, P. Lablanquie, F. Penent, and K. Ito, J. Chem. Phys. **138**, 214308 (2013).
[11] R. Takai, T. Obina, Y. Tanimoto, T. Honda, M. Shimada, Y. Kobayashi, and T. Mitsuhashi, Proc. IPAC **10**, 2564 (2010).
[12] K. Amemiya, A. Toyoshima, T. Kikuchi, T. Kosuge, K. Nigorikawa, R. Sumii, and K. Ito, AIP Conf. Proc. **1234**, 295 (2010).

[13] J. Adachi *et al.* (unpublished).
[14] J. H. D. Eland, O. Vieuxmaire, T. Kinugawa, P. Lablanquie, R. I. Hall, and F. Penent, Phys. Rev. Lett. **90**, 053003 (2003).
[15] K. Ito, F. Penent, Y. Hikosaka, E. Shigemasa, I. H. Suzuki, J. H. D. Eland, and P. Lablanquie, Rev. Sci. Instrum. **80**, 123101 (2009).
[16] G. C. King, M. Tronc, F. H. Read, and R. C. Bradford, J. Phys. B: At. Mol. Phys. **10**, 2479 (1977).
[17] P. Lablanquie, L. Andric, J. Palaudoux, U. Becker, M. Braune, J. Viefhaus, J. H. D. Eland, and F. Penent, J. Electron Spectrosc. Relat. Phenom. **156–158**, 51 (2007).
[18] NIST Atomic Spectra Database (ver. 5.3) online: http://physics.nist.gov/asd